

Molecular beam scattering of NO+Ne: A joint theoretical and experimental study

Y. Kim and H. Meyer

Department of Physics and Astronomy, The University of Georgia, Athens, Georgia 30602-2451

M. H. Alexander

Department of Chemistry and Biochemistry, The University of Maryland, College Park, Maryland 20742-2021

(Received 2 February 2004; accepted 26 April 2004)

The collision dynamics of the NO+Ne system is investigated in a molecular beam scattering experiment at a collision energy of 1055 cm^{-1} . Employing resonance enhanced multiphoton ionization of NO, we measured state-resolved integral and differential cross sections for the excitation to various levels of both spin-orbit manifolds. The dependence of the scattered intensity on the laser polarization is used to extract differential quadrupole moments for the collision induced angular momentum alignment. The set of cross section data is compared with results of a full quantum mechanical close coupling calculation using the set of *ab initio* potential energy surfaces of Alexander *et al.* [J. Chem. Phys. **114**, 5588 (2001)]. In previous work, it was found that the positions and rotational substructures for the lowest bend-stretch vibrational states derived from these surfaces agree very well with the observed spectrum of the NO–Ne complex. For the same potential, we find that the calculated cross sections show a less satisfactory agreement with the experimental data. While the overall J_f dependence and magnitude of the integral and differential cross sections are in good agreement, noticeable discrepancies exist for the angle dependence of the differential cross sections. In general, the calculated rotational rainbow structures are shifted towards larger scattering angles indicating that the anisotropy of the potential is overestimated in the fit to the *ab initio* points or in the *ab initio* calculation itself. For most states, we find the measured alignment moments to be in excellent agreement with the results of the calculation as well as with predictions of sudden models. Significant deviations from the sudden models are observed only for those fine-structure changing collisions which are dominated by forward scattering. Results of the full quantum calculation confirm the deviations for these states. © 2004 American Institute of Physics. [DOI: 10.1063/1.1763149]

I. INTRODUCTION

In recent years, the interaction of open shell molecules and different rare gas atoms has been studied in great detail.^{1–5} Systems involving the radicals OH or NO and their interaction with different rare gases have evolved as prototypical examples. In particular, the bound state spectroscopy of NO–Ar and OH–Ar complexes has provided much detail about the intermediate and long-range parts of the interaction.^{6–14} The interaction at short range, especially for the NO–Ar system, has been probed in numerous molecular beam scattering experiments.^{15–27} Also the collision dynamics with He has been studied extensively.^{27–34}

There have been fewer investigations of the NO–Ne system. Several early scattering probes of the interaction potential were limited to the determination of integral and differential cross sections without state resolution.^{35,36} More recently, we reported a spectroscopic investigation of the lowest bend-stretch vibrational states of the NO–Ne complex.³⁷ The observed positions and rotational substructures of the measured bands were in excellent agreement with predictions based on a set of high level *ab initio* potential energy surfaces (PESs).³⁸ Analysis suggested only very small deficiencies of the potential in the well region.

The incomplete recovery of the correlation energy for these weakly bound complexes causes the well of the potential to be too shallow and located at slightly too large a NO–Rg distance. This results in a rotational constant that is too small. Discrepancies in the NO–Ne ω splitting also suggest small deficiencies in the average potential.³⁹ The *P*-type doubling, which involves the difference potential,³⁹ is predicted slightly too small. Despite these small discrepancies, the potential predicts most of the observed features correctly. In fact, many of the NO–Ne rotational structures could be reliably assigned only by using the results of the *ab initio* calculation as a guide. This and our earlier study of NO–Ar complexes¹⁴ suggest that high-level *ab initio* calculations of potential surfaces combined with full quantum dynamics calculations provide an extremely accurate description of the spectroscopy of the NO–noble gas complexes.

We might ask if similar accuracy can be obtained for NO–noble gas scattering dynamics. For the NO–Ar system, a series of imaging studies^{24–26} indicate that calculations based on high-quality *ab initio* PESs can provide nearly quantitative predictions (at least relative predictions) of the experimental differential cross sections. We here report a similar comparison for the scattering of NO by Ne. State-

resolved integral and differential cross sections are measured in a counterpropagating molecular beam scattering experiment. A complete set of cross section data is compared with the results of a close coupling calculation using the *ab initio* PESs of Soldan and Wright.³⁸

We also report differential alignment moments of the final angular momentum distribution. In the past, we measured quadrupole moments of the angular momentum distribution for collisions of NH₃ and CO with He or H₂.^{40–43} In all cases, the observed differential alignment was in excellent agreement with predictions of the sudden kinematic apse (KA) or the geometric apse (GA) models proposed by Khare *et al.*⁴⁴ The assumption of an instantaneous angular momentum transfer implies that the projection of the rotational angular momentum onto the direction of linear momentum transfer is conserved in the collision. Since this model does not invoke any interaction potential, observed deviations from this sudden limit can provide information about details of the underlying interaction.

There are two possible origins of a breakdown of the sudden assumption: First, inelastic cross sections dominated by forward scattering are usually sensitive to the weak, long-range part of the interaction which acts over a considerable distance. Second, cross sections involving simultaneous energy transfer into other degrees of freedom besides rotation are likely to cause deviations from the sudden limit. This latter case can occur in collisions involving NO since two types of rotationally inelastic transitions are possible: fine-structure conserving and fine-structure changing. Since the latter are governed by the difference between the two NO–noble gas PESs,⁴⁵ deviations from a simple sudden model are more likely. From an experimental point of view the detection of alignment in a collision process is already a major challenge. To detect any deviations from the sudden limit requires extremely accurate intensity measurements. However, recent improvements in our experimental setup as well as the availability of *ab initio* PESs and the feasibility of a full quantum mechanical treatment of the dynamics make NO+Ne an ideal model system.

The paper is organized as follows: In the following section, we present details of the CC calculation of the different types of cross sections. Section III provides a summary of the experiment and the procedures used for the extraction of center-of-mass (c.m.) cross sections from the experimental data. Theoretical and experimental cross sections are compared and discussed in Sec. IV. We end with a brief conclusion.

II. CLOSE COUPLED SCATTERING CALCULATIONS

The approach of a structureless atom to a molecule in a ²Π electronic state gives rise to two PESs, of A'' and A' symmetry with respect to reflection in the triatomic plane. The PESs are a function of the three Jacobi coordinates used to describe the triatomic system: *r* (the NO bond distance), *R* (the distance between the Ne atom and the center of mass of the NO molecule), and *θ* (the angle between \vec{r} and \vec{R}). In the calculations presented here, as in our investigation of the NO–Ne complex, we use the *ab initio* PESs of Wright and

Lee, and subsequently fitted by Soldan.³⁸ These were determined by restricted coupled-cluster [RCCSD(T)] calculations with a large basis set and with the NO bond distance held fixed at 1.1526 Å [the equilibrium internuclear separation predicted by a comparable RCCSD(T) calculation on the isolated NO molecule].

In the treatment of the scattering,^{12,39,45,46} it is convenient to work with the average and half difference of the PESs for the states of A'' and A' reflection symmetry, defined as

$$V_{sum} = \frac{1}{2}(V_{A''} + V_{A'})$$

and

$$V_{dif} = \frac{1}{2}(V_{A''} - V_{A'}).$$

Full close-coupled scattering calculations involving both potential surfaces were carried out at total energies of 1160, 1040, and 940 cm⁻¹. These energies span the range of collision energies sampled in the scattering experiments, as described in the following section. To obtain convergence in the scattering calculations, all rotational levels with *J*'_f ≤ 24.5 (26.5 for the calculations at 1160 cm⁻¹) were included in the expansion of the scattering wave function, and all values of the total angular momentum ≤ 130.5 were included. The calculations were carried out with the HIBRIDON program suite.⁴⁷

III. EXPERIMENT AND DATA ANALYSIS

Details of the molecular beam apparatus have been described previously.^{48,49} Briefly, two pulsed molecular beam sources are mounted in a 500 mm diameter source chamber pumped by an 11 000 l/s diffusion pump. This chamber also contains the differentially pumped scattering chamber evacuated by a 3000 l/s diffusion pump. Both diffusion pumps are backed by a single roots-rotary pump combination. The molecular beam pulses enter the scattering chamber through skimmers on opposite walls of the scattering chamber. Tunable UV light for ion detection through resonance enhanced multiphoton ionization (REMPI) is generated with a Nd:YAG (YAG–yttrium aluminum garnet) pumped dye laser system operating at a repetition rate of 10 Hz. The output of the dye laser is frequency doubled in a potassium dihydrogen phosphate (KDP) crystal. About 1 mJ/pulse of UV radiation is focused onto the molecular beam with a 500 mm lens. The linear laser polarization is controlled with a laser *Q* switch (Cleveland Crystals) to be either parallel or perpendicular to the molecular beam axis. Ions generated by the focussed laser beam are accelerated in a two-field electrode arrangement. A dispersion field is used to separate the ions according to their velocity component in the direction of the molecular beam. In a second field, the ions are accelerated towards a combination of two electrostatic mirrors which deflect them towards a microchannel plate (MCP) detector (Del Mar Ventures, San Diego, CA). In comparison with the

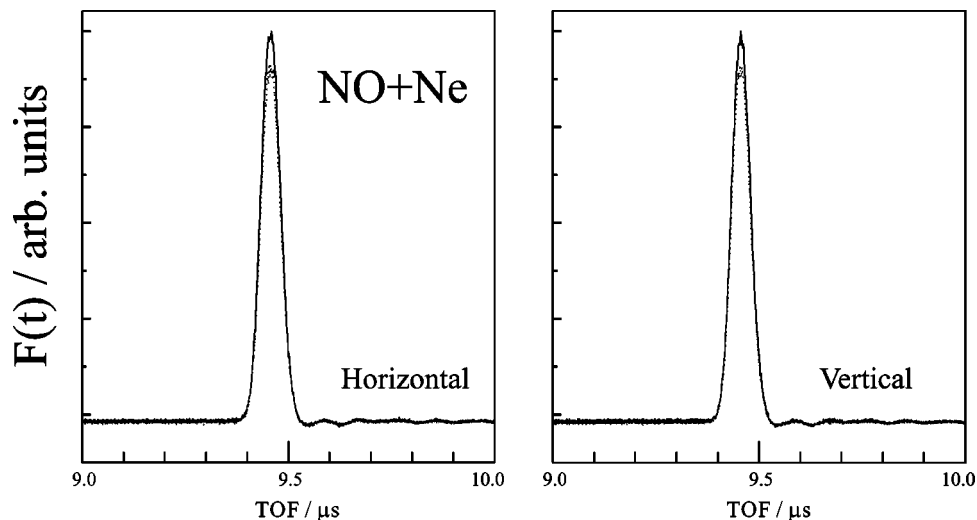


FIG. 1. TOF spectra probing the level $J=0.5$ of NO in the primary beam with (dashed) and without (solid) target beam recorded for the indicated direction of the laser polarization.

original design, this electrode setup provides an improved velocity resolution while maintaining a high detection sensitivity.^{50,51}

The NO beam is generated by expanding a 5% NO/Ar mixture from a home-built piezoelectric valve at a backing pressure of 1.4 bar.⁵² The expansion of NO in Ar results in a rotational temperature of about 2 K consistent with the almost exclusive population of the $J_i=0.5$ level. Both λ doublets are assumed to be equally populated. This assumption is consistent with the resonantly enhanced multiphoton ionization (REMPI) spectrum for the NO molecular beam which yields equal population of the two λ doublets with an uncertainty of about 20%. Note that the λ -doublet components of probed states can be distinguished in the (2+1) REMPI detection step. The next higher energy level corresponding to $J=1.5$ is reduced in intensity by a factor of at least 20. The target beam is generated by expanding Ne from a commercial molecular beam valve (JORDAN CO) at a backing pressure of 1.6 bar. The two pulses have a duration [full width at half maximum (FWHM)] of about 60 μs . The most probable velocities in the beams are 610 m/s for NO in Ar and 840 m/s for the Ne beam resulting in a collision energy of $1055 \pm 75 \text{ cm}^{-1}$.

Different final states of NO are probed using (2+1) REMPI detection via the Rydberg state $\text{H}^2\Sigma, \text{H}'^2\Pi$.⁵³ Details of the spectroscopy and its application towards the detection of aligned product ensembles have been presented recently.⁵⁴ Although the spectrum is dominated by a zeroth rank tensor component of the two-photon absorption operator, the presence of small second rank tensor components is responsible for a pronounced polarization dependence of the signal if an aligned molecular ensemble is probed.

A. NO depletion

In a counterpropagating molecular beam scattering experiment, the scattering volume depends critically on the relative delay of the two molecular beam pulses. The delay directly determines the overlap and thus the effective scatter-

ing length. In order to assess the probability for multiple collisions, we carefully monitor the depletion of the NO initial state. In Fig. 1, we display time-of-flight (TOF) spectra measured with the indicated laser polarization. From the difference of spectra taken with and without target beam, we deduce a depletion of $D=0.08$ for both λ -doublet components independent of the laser polarization. Assuming a minimum mean free path of 25 cm corresponding to a particle density of $10^{13}/\text{cm}^3$ and a total cross section of 40 \AA^2 in combination with a pulse overlap of 2 cm, we find the following estimates for multiple collisions calculated for a Poisson distribution: 8% single collisions and 0.3% secondary collisions. The observed depletion reflects the sum of the integral cross sections over all final states for the probed λ -doublet component of the initial level with $J_i=0.5$. For the analysis of the integral cross section data and the TOF spectra, we must take into account the depletion of the rest population in different final states. Although the total cross section for the depletion of different final states can in principle vary as a function of J_f , we assume $D_f=0.08$ independent of J_f .

B. Integral cross sections

Integral cross sections (ICS) are measured using a base line subtraction mode which allows us to discriminate the signal due to scattering into a final state from a possible rest population of the state of interest. The background subtraction is accomplished by pulsing the target molecular beam source at half the repetition rate of the laser and measuring the detector signal simultaneously with two identical boxcar averaging systems. One boxcar averager operates in a base line subtraction mode acquiring the difference signal T_f associated with two consecutive pulses while the other boxcar operates in the standard averaging mode yielding a signal S_f . Care is taken that the gates of both boxcars yield identical signals when operated in the standard averaging mode. Spectra are measured as a function of the laser frequency with the laser polarization parallel to the molecular beam axis. In order to increase the signal-to-noise ratio in these measurements, we use a single electric field of 100 V/cm for

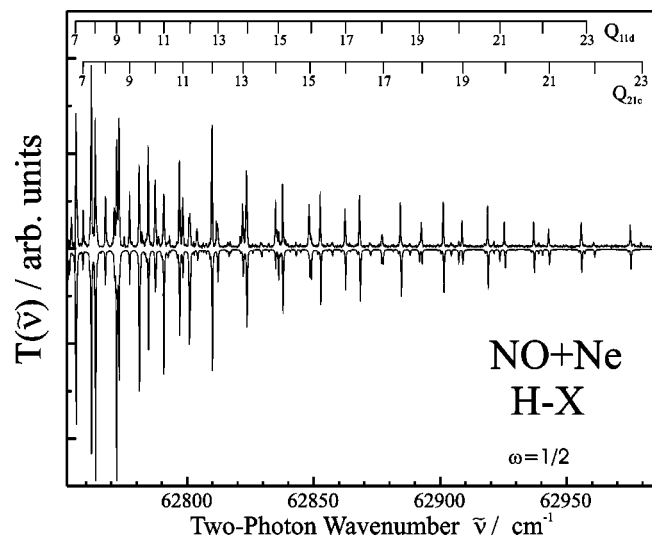


FIG. 2. Scattering signal in the frequency region probing fine-structure conserving collisions. The rotational lines belonging to the branches Q_{11d} and Q_{21c} are marked with $(J_f - 0.5)$.

the acceleration of the ions towards the detector. Even with the resulting signal enhancement, it was not feasible to measure the polarization dependence of the integral scattering signal because of the extensive averaging required. Using a 30 shot average, we estimate the experimental uncertainty to be less than 30% for the smallest cross sections. Values of T_f and S_f for individual final states are determined in a fit to the spectra taking into account the line strength of individual transitions. Because most final states can be probed on lines of different Q branches, the individual results are averaged. In the excited state, the spin-uncoupling operator is responsible for a strong J -dependent perturbation affecting levels of type $1d$ and $2c$.⁵⁴ These perturbations are responsible for anomalous line strengths and level spacings. In particular, levels with values of J near 5.5 are affected. The Q -branch lines that involve these perturbed levels are labeled with $(J \cdot 0.5)$ in Figs. 2 and 3. As a consequence, intensities of these lines are not as well reproduced in the fit as lines belonging to the unperturbed branches. Typical spectra of type T_f are displayed in Figs. 2 and 3 for different types of fine-structure transitions.

The rest population $n_f(rst)$ and the population transfer Δn_f are extracted from the signals T_f and S_f taking into account the depletion of the rest population due to scattering from the target beam:⁴⁸

$$\Delta n_f = (1 - \frac{1}{2} D_f) T_f + D_f S_f, \quad (1a)$$

$$n_f(rst) = S_f - \frac{1}{2} T_f. \quad (1b)$$

As a result of the supersonic expansion, NO is cooled rotationally extremely efficiently, and the population transfer Δn_f is approximately proportional to a laboratory ICS I_{lab} for scattering from the initial level into the final state f . Obviously, this cross section represents the average over the different initial states including the two λ -doublet components. In the following, we neglect the small contamination due to the 5% population of the $J=1.5$ level.

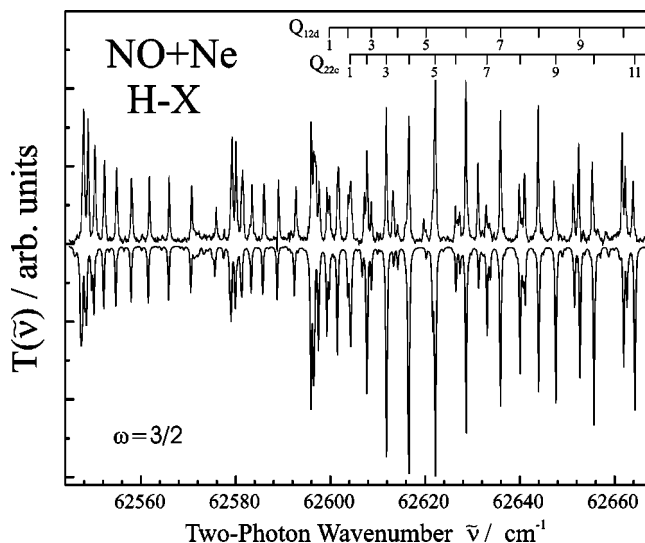


FIG. 3. Scattering signal in the frequency region probing fine-structure changing collisions. The rotational lines belonging to the branches Q_{12d} and Q_{22c} are marked with $(J_f - 0.5)$.

In the counterpropagating molecular beam setup, the detection efficiency is not necessarily uniform. In most cases, particles scattered either into the forward or into the backward directions are detected more efficiently. Therefore, the experimentally determined scattered intensity represents a laboratory ICS I_{lab} which must be distinguished from the true ICS denoted I_{cm} . A proper comparison of I_{lab} with theoretical data involves the convolution of the theoretical differential cross section (DCS) with an apparatus function that describes the correlation between scattering angle and the projection of the final velocity onto the molecular beam axis. Most importantly, this function describes the velocity- and, therefore, angle-dependent detection efficiency.^{48,51} In Fig. 4 we show the relative ratio of I_{lab} and I_{cm} based on the results of the CC calculation as a function of the energy transfer

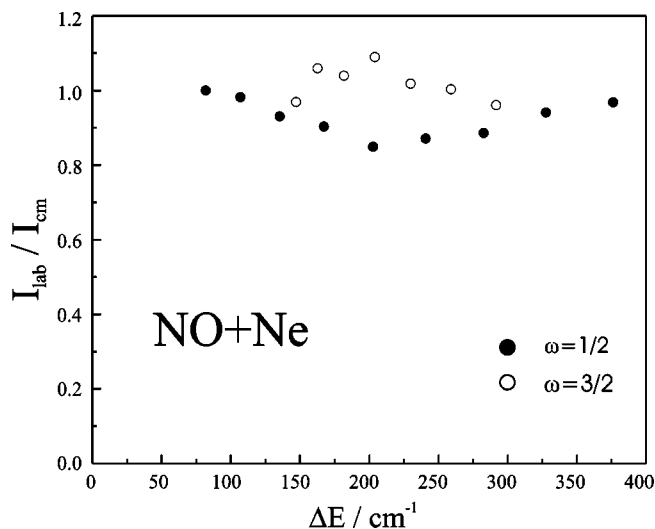


FIG. 4. Normalized ratio of the calculated laboratory and true ICS as a function of the energy transfer ΔE .

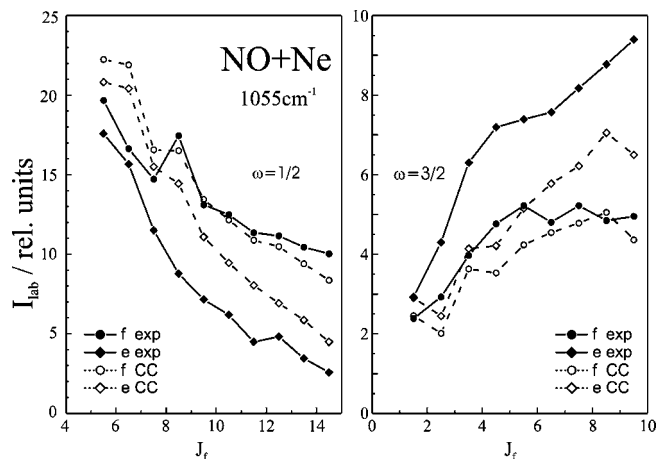


FIG. 5. Experimental and theoretical laboratory ICSs for the indicated fine-structure conserving collisions (right panel) and fine structure changing collisions (left panel) as a function of J_f .

ΔE . The ratio varies by almost 20% for the NO+Ne system. The variations reflect the angle dependence of the detection efficiency and the DCS. For example, fine-structure conserving transitions favor large angle scattering with increasing energy transfer. Since sideways scattering is detected with lower sensitivity, the corresponding cross section I_{lab} is reduced causing the minimum of the ratio for energy transfers near 200 cm^{-1} . DCSs corresponding to larger energy transfers are dominated by backward scattering resulting in the relative increase of the laboratory ICS. Obviously, the same argument applies to the cross sections for fine-structure changing collisions. The laboratory ICSs for the population of different λ doublets in both spin-orbit manifolds are displayed in Fig. 5. For a meaningful comparison between the theoretical and experimental data we determine an overall scaling factor that minimizes the differences between the two sets. The scaled experimental ICSs are used to normalize the experimental TOF spectra. This not only allows us to compare directly theoretical and experimental TOF spectra but also the corresponding DCSs.

C. Differential cross sections and alignment

TOF spectra for different final states of NO are measured in the velocity dispersion mode: dispersion field 5 V/cm and acceleration field 70 V/cm . Many of the final states probed show a small but significant rest population due to the incomplete rotational cooling of NO in the expansion. We distinguish the rest population from the scattering signal by determining the difference of two TOF spectra: One measured with the target beam overlapping and the other with the target beam missing the NO beam pulse. In order to generate a TOF spectrum representing the scattering into a particular final state, we subtract the spectrum due to the rest population taking into account the depletion of the latter. The dependence on the laser polarization is determined by measuring pairs of spectra $F_h(t)$ and $F_v(t)$ with the laser polarization parallel and perpendicular to the molecular beam axis. For each setting of the laser polarization and the target beam delay, 500 TOF spectra are averaged with a digi-

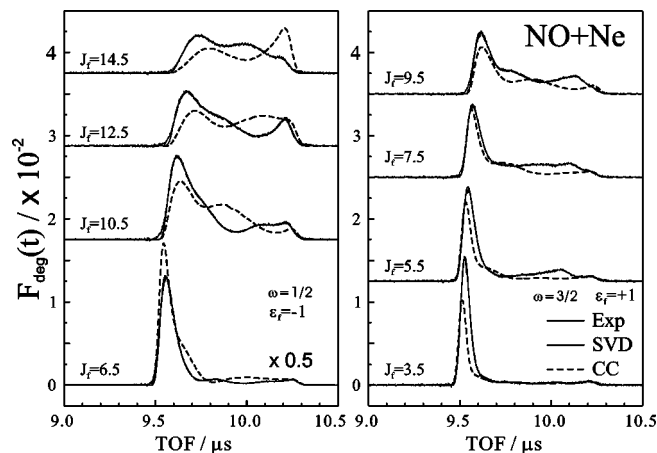


FIG. 6. Degeneracy averaged TOF spectra for the indicated final states. Spectra probing levels with $(\omega=0.5, \epsilon_f=-1)$ are recorded on lines of the Q_{21d} branch while spectra probing levels $(\omega=1.5, \epsilon_f=+1)$ are recorded on the Q_{12s} branch. All spectra are displayed on the same relative scale consistent with the integral cross sections of the figure.

tal oscilloscope whose output is subsequently transferred to a PC for storage and further analysis. In this way, we simultaneously build up polarization dependent TOF spectra avoiding long term drifts in the laser power or the molecular beam densities. From the TOF spectra associated with the two different settings of the laser polarization, we generate a degeneracy averaged spectrum $F_{deg} = \frac{1}{3}(F_h + 2F_v)$ and a difference spectrum $F_{diff} = F_h - F_v$. Examples of these types of TOF spectra for fine-structure conserving and changing collisions are shown in Figs. 6 (degeneracy averaged) and 7 (difference).

DCSs are extracted from the TOF spectra with the help of an apparatus function $\tilde{G}(v_{fz}, \cos \theta)$ which is determined from the scattering kinematics, the characteristics of the molecular beam pulses, and the relative delays of all pulses.^{49,51} $\tilde{G}(v_{fz}, \cos \theta)$ describes the correlation of the projection v_{fz} of the final laboratory velocity vector with $\cos \theta$ where θ represents the scattering angle in the c.m. frame. The incorporation of the different delays defines an effective scattering

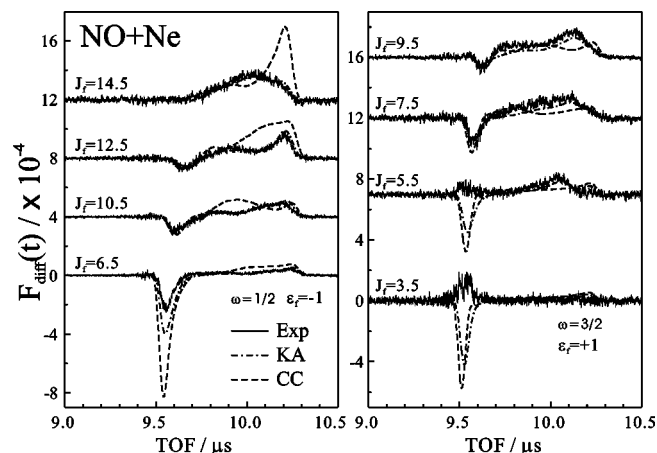


FIG. 7. Difference TOF spectra for the indicated final states. The spectra are displayed on a relative scale consistent with the integral cross sections of Fig. 5.

volume through the spatial and temporal profiles of the molecular beam pulses and assures that $\tilde{G}(v_{fz}, \cos \theta)$ describes correctly the delay dependence of the scattered intensity. The apparatus function is defined in such a way that the velocity distribution $\tilde{F}(v_{fz})$ associated with a TOF spectrum $F(t)$ is related to the DCS $\sigma(\cos \theta)$ through a simple convolution:

$$\tilde{F}(v_{fz}) = \int_{-1}^1 d \cos \theta \tilde{G}(v_{fz}, \cos \theta) \sigma(\cos \theta). \quad (2)$$

Because we normalize the area of experimental TOF spectra to the measured laboratory ICSs which in turn are scaled to the set of theoretical ICSs, the extracted DCSs have the correct relative magnitude allowing us to compare them among each other but also with theoretical DCSs. Here we assume that the different apparatus functions are normalized in a consistent manner; for example, by using the same grid for the calculation: 100 points in v_{fz} and 30 points in $\cos \theta$. Because the radius of the Newton sphere decreases with increasing energy transfer, the effective angular resolution is lowered accordingly. For some final states, the reduced resolution causes an unphysical oscillatory behavior of the DCS when applying a simple linear least squares fitting procedure. These difficulties are avoided by applying the method of single value decomposition (SVD) for the determination of the DCS.⁵¹

From the analysis of the polarization dependent TOF spectra, we find the degeneracy averaged cross section $\sigma_{deg}(\cos \theta)$ and a difference cross section $\sigma_{diff}(\cos \theta)$. The latter can be used to derive the differential quadrupole moment $T_0^{(2)}(\cos \theta)$ of the angular momentum distribution

$$\frac{\sigma_{diff}(\cos \theta)}{\sigma_{deg}(\cos \theta)} = 3 \frac{\sqrt{2J''+1} B_2(J'', J')}{2 B_0(J'', J')} T_0^{(2)}(\cos \theta). \quad (3)$$

The coefficients B_0 and B_2 must be calculated from the angular momenta, the electronic wave functions and the matrix elements involved in the two-photon transition. For the H-X transition, details are discussed in Ref. 54. The alignment moments $T_k^{(Q)}$ are defined by Blum.⁵⁵ They are directly proportional to the moments $A_k^{(Q)}$ defined by Greene and Zare.⁵⁶ Since the quadrupole moment involves the ratio of two quantities with rather large experimental uncertainty, we expect a corresponding error in the derived alignment moment. Nevertheless, the resulting data can be compared directly with the results of the CC calculation.

As will be shown in the following section, many of the observed alignment characteristics can be understood in terms of a sudden collision. The validity of these models is best checked against experimental data by comparing difference TOF spectra based on the velocity distribution,

$$\tilde{F}_{diff}(v_{fz}) = \int_{-1}^1 d \cos \theta \tilde{G}(v_{fz}, \cos \theta) \sigma_{diff}(\cos \theta). \quad (4)$$

Here $\sigma_{diff}(\cos \theta)$ is calculated according to Eq. (3). In the case of the sudden models, we use the experimentally determined degeneracy averaged DCS in the calculation of $\sigma_{diff}(\cos \theta)$. Therefore, any deviation in the difference spectrum can be attributed to the failure of the models. Furthermore, we can check how the next higher-order state multi-

pole moment, i.e., $T_0^{(4)}$, affects an alignment measurement based exclusively on the use of horizontal and vertical laser polarization. Using the predictions of the sudden models, we find that the difference spectra are completely dominated by the quadrupole moment. For some final states contributions due to $T_0^{(4)}$ can be recognized although they usually are within the experimental noise.⁵¹ In this context it is important to emphasize that the moment $T_0^{(4)}$ predicted by the sudden models is in very good agreement with the results of the CC calculation.

IV. RESULTS AND DISCUSSION

The measured integral cross sections for fine-structure conserving and changing collisions are compared with the theoretical values determined for $E_{col} = 1040 \text{ cm}^{-1}$ in Fig. 5. The four sets of experimental cross sections were scaled with a single factor in order to best match the theoretical values. Although the estimated experimental error is in the order of $\pm 15\%$, we find qualitative agreement for all cross sections. The relative magnitudes of the spin-orbit conserving cross sections, and their variation with the final rotational quantum number is predicted well. However, the predicted integral cross sections for the spin-orbit changing cross sections are too small. This suggests that the difference potential is too small in the region probed in the scattering experiment. Interestingly, the comparison of the bound states suggested a similar discrepancy for the well region. In this case, we found the *P*-type doubling and, in particular, its *J* dependence to be noticeably underestimated by the *ab initio* potential.³⁸

We also observe a marked propensity for excitation of λ doublets corresponding to rotational levels with A'' electronic symmetry⁵⁷ [the *f* levels ($\epsilon = -1$) in the $\omega = 1/2$ spin-orbit manifold and the *e* levels ($\epsilon = +1$) in the $\omega = 3/2$ spin-orbit manifold]. This is seen in both the experimental and theoretical cross sections. This propensity is more pronounced in the experimental data. This propensity has its origin in the spin-uncoupling contribution to the diatom Hamiltonian causing the mixing of different Hund's case (a) basis states as the value of J_f increases.⁴⁶ The excitation into *f*-labeled levels is predicted almost quantitatively for both spin-orbit components. However, the calculated cross sections for transitions into the *e*-labeled levels are too large in the case of fine-structure conserving collisions and too small for fine-structure changing collisions. If the NO molecule were pure Hund's case (a), then the spin-orbit changing transitions would be governed solely by the difference potential.⁴⁵ Further, the cross sections would be independent of the symmetry index of the final state. The large difference between the cross sections into the *e* and *f* levels reflects quantum interference between the sum and difference potentials.⁵⁸ The discrepancies seen in Fig. 5 between the predicted and measured A'' to A' ratios suggest that small errors in the difference PESs may be amplified by this interference effect.

Degeneracy averaged TOF spectra calculated from the theoretical DCSs are shown as dashed lines in Fig. 6 together with the experimental data. The underlying DCSs are com-

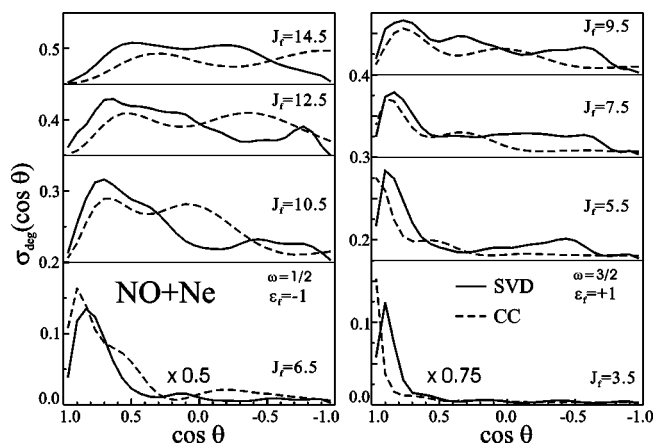


FIG. 8. Degeneracy averaged differential cross sections for the fine-structure conserving (left panel) and fine-structure changing (right panel) collisions. All cross sections are shown on the same relative scale established through the integral cross sections.

pared in Fig. 8. Again we find good agreement for the overall shape of the DCSs. Both sets of cross sections show an increased probability for large angle scattering with increasing J_f . Comparing the J_f dependence of cross sections corresponding to $\Delta\omega=0$ and $\Delta\omega=+1$, we notice a similar angular dependence although the fine structure changing collisions involve a considerably larger energy transfer for a given value of J_f . This trend is also predicted by the theoretical calculation.

A closer inspection of the TOF spectra as well as the DCSs reveals several pronounced maxima. These correspond to rotational rainbows.⁵⁹ Both experiment and theory reveal that these maxima are shifted towards larger scattering angles with increasing ΔJ . For fine-structure conserving collisions, the calculation predicts several maxima. With increasing J_f , one maximum is shifted from forward scattering to $\cos\theta=0.5$ while a second maximum is shifted towards backward scattering. For $J_f=6.5$, a shoulder in the forward peak marks the position of the second maximum while, for $J_f=7.5$ (see Fig. 9), this maximum is separated from the forward peak and a third maximum is observed at $\cos\theta=-0.5$. In general, we observe the third maximum for low values of J_f near $\cos\theta=-0.3$. Similar structures are also observed in the experimental spectra. At the smallest values

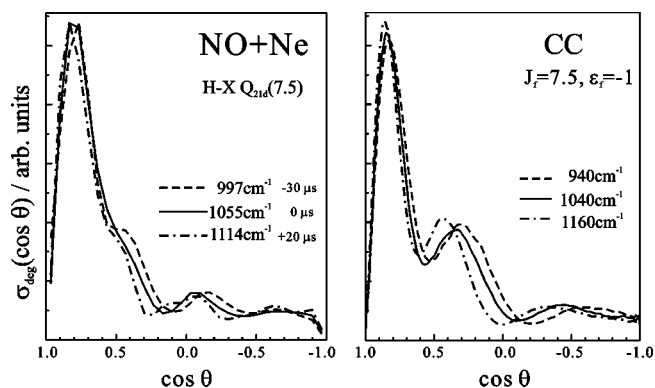


FIG. 9. DCS for the excitation of the level $(\omega, J_f, \epsilon_f) = (0.5, 7.5, -1)$ for the indicated collision energies: Experiment (left panel) and CC (right panel).

of J_f , we observe a maximum for forward scattering with a secondary maximum discernible as a shoulder at slightly larger scattering angles. A third structure is observed for $\cos\theta=0$. With increasing J_f the structures are also shifted towards larger angles. In contrast to the results of the theoretical calculation, the shifts are considerably smaller. As a result, experimental TOF spectra or the associated cross sections for a particular value of J_f agree well in shape with theoretical data corresponding to a lower value of J_f . For example, the general angular dependence of the experimental data for $J_f=7.5, 12.5$, and 14.5 agree better with the predicted cross sections for $J_f=6.5, 10.5$, and 12.5 , respectively. We note that similar rainbow structures, and similar shifts to larger angles with increasing J_f were seen in the recent molecular beam/imaging experiments on collisions of NO with Ar.^{24–26}

A similar situation is found for fine-structure changing collisions. For example, we find good agreement in the angular position of the structures in the experimental spectrum for $J_f=9.5$ with the structures predicted for $J_f=7.5$. We also notice a broad maximum in the experimental data for $J_f > 4.5$ and scattering angles with $\cos\theta < -0.5$ which is absent in the theoretical prediction. Nevertheless, this maximum shows the characteristic shift towards larger scattering angles with increasing J_f confirming that it is not an artifact, for example, due to spectroscopic congestion.

To investigate further the observed discrepancies in the position of the maxima, we looked at the effect of varying the center-of-mass collision energy. Although we could not vary this over a wide range, we were able to measure TOF spectra for $J_f=7.5$ using different delays within the FWHM center of the target molecular beam pulse. For these delays, collisions result from different regions in the center of the target beam pulse. As shown in Ref. 50, the local velocity distribution in the central part of the pulse as measured through ion TOF analysis does not change significantly in width while the local most probable velocity changes noticeably. Furthermore, Monte Carlo simulations of the scattering kinematics reveal that the scattered flux contributing to a TOF spectrum is generated in a small volume near the laser focus extending ± 5 mm along the molecular beam axis. For comparison, the spatial width of the target beam pulse (FWHM) is 50 mm. As a result the applied target beam delay variations result in small changes in the average collision energy of about ± 60 cm^{-1} without changing its spread. The measured spectra are analyzed with an apparatus function appropriate for the relative delay and for the velocity distribution of the target beam. The resulting DCSs are displayed in the left panel of Fig. 9. Although the cross sections are almost identical, we notice small but significant shifts in the position of the observed structures; most noticeably for the shoulder at $\cos\theta=0.4$ and the maximum near $\cos\theta=-0.1$. In the right panel of Fig. 9, we display the results of the CC calculation for three collision energies. Again the structures in the DCS exhibit a very similar dependence on the collision energy. In both sets of data, the structures shift towards smaller scattering angles with increasing collision energy. The larger shifts in the theoretical cross sections are attrib-

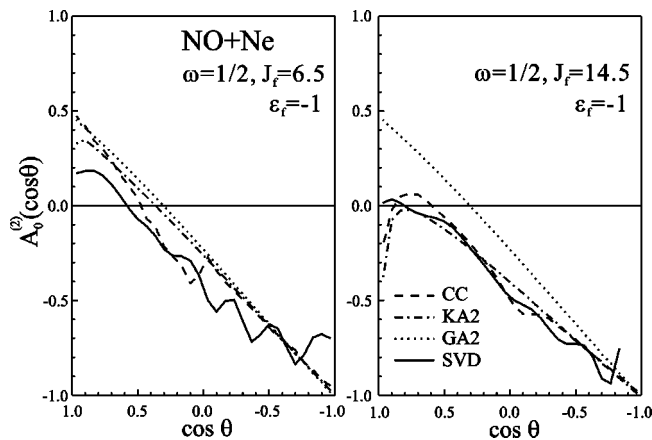


FIG. 10. Differential quadrupole moments for the indicated final states. The experimental result is shown as solid line while the predictions of the sudden models are represented as dashed curves. The result of the CC calculation is given as the dotted line.

uted to the larger variation in the collision energy in the calculations (+120 and -100 cm^{-1}).

Overall, theory predicts an energy dependence very similar to that seen experimentally. However, the degree of variation is not enough to explain the differences seen in the position of the maxima, when the theoretical and experimental DCSs are compared.

The position of the rotational rainbow maxima can be related to the anisotropy of the interaction potential. Within the framework of a classical hard ellipsoid model, the rotational rainbow positions are related to the eccentricity of the ellipsoid.⁶⁰ If we identify the efficiency for angular momentum transfer as being reflected by the anisotropy of the average potential, if we assume that the spin-orbit conserving transitions can be approximated by hard ellipsoid scattering on a single PES, then we might infer that the effective anisotropy of the average potential is overestimated by the *ab initio* calculations.

According to Eq. (3), difference cross sections or difference TOF spectra involve the quadrupole moment of the dependence of the inelastic cross sections on the projection quantum number of the final rotational state, as well as the degeneracy averaged cross section. Since both quantities are available from the CC calculation, we compare in Fig. 7 the theoretical difference TOF spectra with the experimental ones. Except for transitions into low J values belonging to the upper spin-orbit manifold, we find very similar polarization effects. The polarization effect changes from negative values for forward scattering to positive values for backward scattering. On the other hand, a reversed sign is observed at small scattering angles for fine structure changing collisions with the lowest values of J_f . Obviously, we cannot expect quantitative agreement because of the discrepancies already noted in the degeneracy averaged cross section. In order to assess differences due to the quadrupole moment itself, we derive experimental values for the quadrupole moments according to Eq. (3). In Figs. 10 and 11, we compare directly different quadrupole moments. For fine-structure conserving collisions, we find excellent agreement between the experimental and theoretical data. Similar agreement is found also

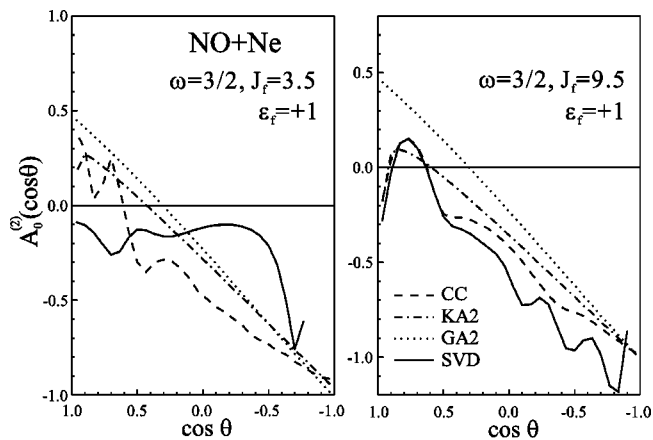


FIG. 11. Differential quadrupole moments for the indicated final states. The experimental result is shown as the solid line while the predictions of the sudden models, KA and GA, are represented as dash-dotted and dotted curves. The result of the CC calculation is given as the dashed line.

for high J_f values belonging to the excited spin-orbit manifold. In the case of the fine-structure changing collisions that are dominated by forward scattering, we find significant deviations especially for forward scattering.

The general behavior of the differential alignment can be understood in terms of an “apse” sudden model.⁴⁴ The kinematic apse model (KA) is based on the assumption that the angular momentum transfer happens instantaneously at a particular distance, for example, the classical turning point. From the conservation of the total angular momentum, it then follows that the rotational angular momentum transfer $\Delta \vec{J}$ must be perpendicular to the linear momentum transfer $\Delta \vec{p}$: $\Delta \vec{J} = -\vec{r}_0 \times \Delta \vec{p}$. If we use the direction of the linear momentum transfer as the quantization axis, the model implies that the projection quantum number M is well defined in this frame (label KA). Assuming only states with $J_i = 0.5$ are present initially, we find the following state multipole moments for a final state with angular momentum quantum number J_f :

$$T_0^{(Q)}(J_f; KA) = \sum_M (-)^{J-M} \sqrt{2Q+1} \times \begin{pmatrix} J_f & J_f & Q \\ M & -M & 0 \end{pmatrix} \rho_{MM}(J_f) = \sqrt{2Q+1} (-)^{J-1/2} \begin{pmatrix} J_f & J_f & Q \\ \frac{1}{2} & -\frac{1}{2} & 0 \end{pmatrix}. \quad (5)$$

After transforming the multipole moments into a scattering frame (label cm) whose z axis coincides with the molecular-beam axis—which is also the direction of the initial relative velocity vector—and after averaging over the azimuthal angle associated with the direction of the linear momentum transfer, we arrive at the multipole moments referred to the scattering frame (see the Appendix of Ref. 42 for details):

$$T_0^{(Q)}(J_f; \text{c.m.}) = T_0^{(Q)}(J_f; KA) P_Q(\cos \beta)$$

$$\text{with } \cos \beta = \frac{R \cos \theta - 1}{\sqrt{R^2 - 2R \cos \theta + 1}}. \quad (6)$$

Here the quantity R is determined by the relative energy transfer: $R = \sqrt{1 - (\Delta E/E)}$. In the case of backward scattering, i.e., $\cos \theta = -1$, both types of moments are identical for all values of ΔE . In particular, we expect the quadrupole moment to be negative and at its maximum absolute value. A similar situation arises for inelastic events observed in the forward direction. For this case, the KA model again yields the most negative quadrupole moment. This prediction contrasts the results for elastic scattering ($R=1$) in the forward direction. Now, the averaging over the azimuthal angle results in a significantly reduced but positive quadrupole moment.

The predictions of the KA model for small angle scattering contrast with those of the geometric apse (GA) model,⁴⁴ which is based on the assumption of a negligible energy transfer. Both models predict strong negative alignment for backward scattering, but they clearly deviate for small angle scattering. Predictions of the quadrupole moment for both models are also displayed in Figs. 10 and 11.

For transitions with the largest ΔE , the GA model is clearly not appropriate. On the other hand, the KA model is in nearly perfect agreement with experiment and the CC calculations. Only in the case of those fine-structure changing collisions which are dominated by forward scattering, do we find significant deviations between the predictions of the sudden models and the CC calculations. Particularly at small scattering angles, the CC results exhibit several strong oscillations indicative of interference effects. The experimental data show clear deviations from the predictions of the two sudden models. Although the experimental data in this region show an oscillation, the sign and magnitude does not agree with the results of the CC calculation. The situation should be contrasted here with NO-Ar, where the experiments of Chandler, Cline, and their co-workers²⁴ find excellent agreement between the measured orientation (dipole moments) of the projection quantum number and CC calculations based on high-quality *ab initio* PESs.

Although our experimental data represent an average over the two λ doublets associated with the initial level $J_i = 0.5$, it is instructive to compare the calculated parity resolved differential alignment moments with predictions of the sudden model. Examples of the moments $A_0^{(2)}$ and $A_0^{(4)}$ are shown in Figs. 12 and 13 for ω -conserving and ω -changing collisions, respectively.

In the case of fine structure conserving transitions, we find excellent agreement with the predictions of the KA model. Noticeable deviations occur for small angle scattering. As shown clearly by the work of Aoiz and co-workers on NO-Ar, large-impact parameter collisions, which sample the long-range part of the potential, contribute significantly to transitions with low ΔJ .⁶¹ For these transitions the sudden approximation will be least appropriate. Further deviations are noticed for scattering angles near 90° , but only for the transition into one parity level.

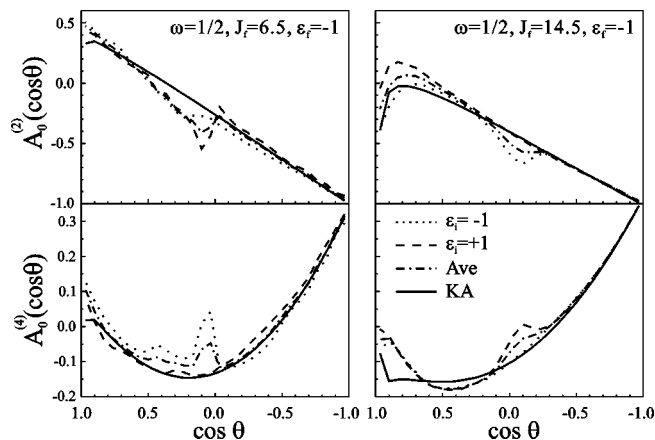


FIG. 12. Comparison of the calculated (CC) differential alignment moments for fine-structure conserving collisions with the predictions of the KA model (solid line). The results of the CC calculation are given as the dashed ($\epsilon_f = +1$), dotted ($\epsilon_f = -1$), and dash-dotted (average) lines.

The situation is different for the moments characterizing fine-structure changing transitions. In this case both types of parity transitions show strong oscillations over a wide range of scattering angles. Although the individual moments show large deviations from the sudden model, in contrast to ω -conserving transitions, parity averaging damps these oscillations (and consequently deviations from the sudden model) except for the smallest ΔJ -transitions.

As a result, we find that for the differential alignment moments $A_0^{(2)}$ and $A_0^{(4)}$ major deviations from the KA model occur mainly for transitions which are governed by the weak long-range interaction, and are therefore not well described as a sudden impact, or for transitions which are sensitive to both PESs, for which the assumption of a single instantaneous angular momentum transfer is invalid.

V. CONCLUSION

The collision dynamics of the NO+Ne system was characterized by measuring and calculating state resolved integral (ICS) and differential (DCS) cross sections as well as

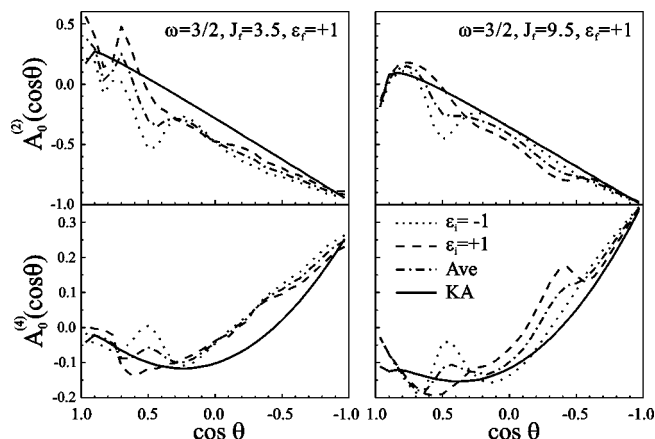


FIG. 13. Comparison of the calculated (CC) differential alignment moments for fine-structure changing collisions with the predictions of the KA model (solid line). The results of the CC calculation are given as the dashed ($\epsilon_f = +1$), dotted ($\epsilon_f = -1$), and dash-dotted (average) lines.

associated alignment moments for a collision energy of 1055 cm^{-1} . The relative magnitude of cross sections for fine-structure conserving and changing collisions is predicted correctly by the calculation based on the *ab initio* potentials of Wright and co-workers.³⁸ The calculations underestimate the magnitude of the fine-structure changing cross sections, which suggests that the calculated difference potential is too small in the region probed in the scattering experiment. This finding is consistent with the earlier analysis of the spectroscopic investigation of the NO–Ne complex,³⁸ where the calculations underestimated the *P*-type doubling.

The experimental and theoretical ICSs show a marked preference for the population of the λ doublet with *A''* symmetry. The fact that this propensity is slightly underestimated in the calculation again is an indication that the difference potential may be too small. The comparison of the angular dependence of the DCS indicates that the effective anisotropy of the potential is too large, most likely for the average potential. The measured collision induced alignment is in excellent agreement with the theoretical calculation and predictions of the sudden model. This simple model breaks down in the case of collisions, which are dominated by the long-range part of the interaction, and for those transitions which sample both potential surfaces. In the latter case, the differential alignment provides an additional probe of nonadiabatic effects in the dynamics.

Overall, the agreement between experiment and theory for the scattering of NO by Ne is less satisfactory than seen in similar comparisons for scattering by Ar.^{24–26} However, the exact opposite is true for the investigations of the bound states of the NO–Ar (Ref. 14) and NO–Ne complexes.³⁸ Here, the CC calculations based on the same *ab initio* PESs were significantly more accurate for the NO–Ne system. Both sets of PESs were determined by similar quality CCSD(T) calculations, and the quantum scattering and bound-state calculations were carried out by an identical close-coupled expansion and formalism. One possible explanation is that the NO–Ne PESs are more accurate than those for NO–Ar in the well region, which is sampled by the bound-state levels. This would seem reasonable, because one can certainly do a better job recovering the correlation energy for a system with fewer electrons.

However, the grid of geometries used to determine the NO–Ne PESs was selected primarily to sample the well region of the potential and was limited to $R > 2.3\text{ \AA}$ = 4.35 bohrs, which is 1.7 bohrs inside the minimum in the *A'* PES. For NO–Ar, by contrast, the grid of geometries extended out from $R = 4.5$ bohrs, which is 2.2 bohrs inside the minimum in the *A'* PES.¹³ In addition, two different techniques were used to fit and extrapolate the PESs. It may well be that the technique used for the NO–Ne system provided a good fit in the region of the well but a less accurate fit (and/or extrapolation) at shorter range, which is probed in the scattering experiments. At collision energies of $\approx 1000\text{ cm}^{-1}$, comparable to the experiments described here, the innermost classical turning point is ≈ 4.9 bohrs.

A further possible deficiency in the NO–Ne (and, similarly, in the NO–Ar) PESs is that they were determined only for a fixed (equilibrium) value of the NO bond distance. In

principle, the full dependence on r should be determined, and then averaged over the ground vibrational wave function of the NO molecule.

It is clear from the present comparison that high-quality scattering experiments, and, in particular, the determination of differential inelastic cross sections and alignments can provide probes of the PESs of weakly interacting systems which are complementary to those provided by spectroscopic experiments on the corresponding weakly bound complexes.

ACKNOWLEDGMENTS

The authors wish to acknowledge the National Science Foundation (Grant No. CHE-0097189 to H.M. and Grant No. CHE-9971810 to M.H.A.) and the donors of the Petroleum Research Fund administered by the ACS for financial support of the research described here.

- ¹M. C. Heaven, *J. Phys. Chem.* **97**, 8567 (1993).
- ²C. C. Carter, H. S. Lee, A. B. McCoy, and T. A. Miller, *J. Mol. Struct.* **525**, 1 (2000).
- ³M. L. Dubernet, D. Flower, and J. M. Hutson, *J. Chem. Phys.* **94**, 7602 (1991).
- ⁴W. H. Green and M. I. Lester, *J. Chem. Phys.* **96**, 2573 (1992).
- ⁵P. J. Dagdigian, in *The Chemical Dynamics and Kinetics of Small Radicals*, edited by K. Liu and A. Wagner (World Scientific, Singapore, 1995).
- ⁶M. T. Berry, M. R. Brustein, J. R. Adamo, and M. I. Lester, *J. Phys. Chem.* **92**, 5551 (1988).
- ⁷C. Chakravarty and D. C. Clary, *J. Chem. Phys.* **94**, 4149 (1991).
- ⁸B. C. Chang, L. Yu, D. Cullin *et al.*, *J. Chem. Phys.* **95**, 7086 (1991).
- ⁹P. D. A. Mills, C. M. Western, and B. J. Howard, *J. Phys. Chem.* **90**, 3331 (1986).
- ¹⁰P. D. A. Mills, C. M. Western, and B. J. Howard, *J. Phys. Chem.* **90**, 4961 (1986).
- ¹¹G. C. Nielson, G. A. Parker, and R. T. Pack, *J. Chem. Phys.* **64**, 2055 (1976).
- ¹²M. H. Alexander, *J. Chem. Phys.* **111**, 7426 (1999).
- ¹³M. H. Alexander, *J. Chem. Phys.* **111**, 7435 (1999).
- ¹⁴Y. Kim, J. Fleniken, H. Meyer, P. J. Dagdigian, and M. H. Alexander, *J. Chem. Phys.* **113**, 73 (2000).
- ¹⁵A. Degli Esposti, A. Bernig, and H. J. Werner, *J. Chem. Phys.* **103**, 2067 (1998).
- ¹⁶M. C. Beck, J. J. ter Meulen, and M. H. Alexander, *J. Chem. Phys.* **113**, 628 (2000).
- ¹⁷H. Thuis, S. Stolte, and J. Reuss, *Chem. Phys.* **43**, 351 (1979).
- ¹⁸P. Casavecchia, A. Lagana, and G. G. Volpi, *Chem. Phys. Lett.* **112**, 445 (1984).
- ¹⁹P. Andresen, H. Joswig, H. Pauly, and R. Schinke, *J. Chem. Phys.* **77**, 2204 (1982).
- ²⁰S. D. Jons, J. E. Shirley, M. T. Vonk, C. F. Giese, and R. W. Gentry, *J. Chem. Phys.* **97**, 7831 (1992).
- ²¹A. G. Suits, L. S. Bontuyan, P. L. Houston, and B. J. Whitaker, *J. Chem. Phys.* **96**, 8618 (1992).
- ²²A. Lin, S. Antonova, A. P. Tsakotellis, and G. C. McBane, *J. Phys. Chem.* **103**, 1198 (1999).
- ²³M. H. Alexander and S. Stolte, *J. Phys. Chem.* **112**, 8017 (2000).
- ²⁴K. T. Lorenz, D. W. Chandler, J. W. Barr, W. W. Chen, G. L. Barnes, and J. I. Cline, *Science* **293**, 5537 (2001).
- ²⁵M. S. Elioff and D. W. Chandler, *J. Chem. Phys.* **117**, 6455 (2002).
- ²⁶H. Kohguchi, T. Suzuki, and M. H. Alexander, *Science* **294**, 5543 (2001).
- ²⁷K. Schreel, J. Schleipen, A. Eppink, and J. J. ter Meulen, *J. Chem. Phys.* **99**, 8713 (1993).
- ²⁸H. Meyer, *J. Chem. Phys.* **102**, 3151 (1995).
- ²⁹M. Yang and M. H. Alexander, *J. Chem. Phys.* **103**, 6973 (1995).
- ³⁰M. Drabells, A. M. Wodtke, M. Yang, and M. H. Alexander, *J. Phys. Chem. A* **101**, 6463 (1997).
- ³¹P. L. James, I. R. Sims, I. M. W. Smith, M. H. Alexander, and M. Yang, *J. Chem. Phys.* **109**, 3882 (1998).
- ³²M. S. Westley, K. T. Lorenz, D. W. Chandler, and P. L. Houston, *J. Chem. Phys.* **114**, 2669 (2001).

- ³³M. H. Alexander, *Faraday Discuss.* **113**, 437 (1999).
- ³⁴J. Klos, G. Chalasinski, M. T. Berry, R. Bukowski, and S. M. Cybulski, *J. Chem. Phys.* **112**, 2195 (2000).
- ³⁵H. Thuis, S. Stolte, J. Reuss, J. J. H. van den Biesen, and C. J. N. van den Meijdenberg, *Chem. Phys.* **52**, 211 (1980).
- ³⁶P. Casavecchia, in *Dynamics of Polyatomic van der Waals Complexes*, edited by N. Halberstadt and K. C. Janda (Plenum, New York, 1990).
- ³⁷Y. Kim, J. Fleniken, and H. Meyer, *J. Chem. Phys.* **114**, 5588 (2001).
- ³⁸M. H. Alexander, P. Soldan, T. G. Wright, Y. Kim, H. Meyer, P. J. Dagdigian, and E. P. F. Lee, *J. Chem. Phys.* **114**, 5588 (2001).
- ³⁹M. H. Alexander, *Chem. Phys.* **92**, 337 (1985).
- ⁴⁰H. Meyer, *Chem. Phys. Lett.* **230**, 519 (1994).
- ⁴¹H. Meyer, *J. Chem. Phys.* **102**, 3110 (1995).
- ⁴²H. Meyer, *J. Phys. Chem.* **99**, 1101 (1995).
- ⁴³H. Meyer, *Mol. Phys.* **84**, 1155 (1995).
- ⁴⁴V. Khare, D. J. Kouri, and D. K. Hoffmann, *J. Chem. Phys.* **74**, 2275 (1981).
- ⁴⁵M. H. Alexander, *J. Chem. Phys.* **76**, 5974 (1982).
- ⁴⁶M. H. Alexander, *J. Chem. Phys.* **99**, 7725 (1993).
- ⁴⁷HIBRIDON is a program package for the time-independent quantum treatment of inelastic collisions and photodissociation written by M. H. Alexander, D. E. Manolopoulos, H.-J. Werner, and B. Follmeg with contributions by P. F. Vohralik, D. Lemoine, G. Corey, B. Johnson, T. Orlikowski, W. Kearney, A. Berning, A. Degli-Esposti, C. Risi, and P. Dagdigian. More information and a copy of the code can be obtained from the website: <http://www.chem.umd.edu/alexander/hibridon>
- ⁴⁸H. Meyer, *J. Chem. Phys.* **101**, 6686 (1994).
- ⁴⁹H. Meyer, *J. Chem. Phys.* **101**, 6697 (1994).
- ⁵⁰Y. Kim, S. Ansari, B. Zwickl, and H. Meyer, *Rev. Sci. Instrum.* **74**, 4805 (2003).
- ⁵¹Y. Kim and H. Meyer, *Chem. Phys.* **301**, 273 (2004).
- ⁵²The original piezoelectric pulsed molecular beam valve was developed in the group of Professor D. Gerlich at the University of Chemnitz, Germany.
- ⁵³H. Meyer, *J. Chem. Phys.* **107**, 7721 (1997).
- ⁵⁴Y. Kim and H. Meyer, *Chem. Phys.* **301**, 283 (2004).
- ⁵⁵K. Blum, *Density Matrix Theory and Applications* (Plenum, New York, 1981).
- ⁵⁶C. H. Greene and R. N. Zare, *J. Chem. Phys.* **78**, 6741 (1983).
- ⁵⁷M. H. Alexander, P. Andresen, R. Bacis *et al.*, *J. Chem. Phys.* **89**, 1749 (1988).
- ⁵⁸P. J. Dagdigian, M. H. Alexander, and K. Liu, *J. Chem. Phys.* **91**, 839 (1989).
- ⁵⁹R. Schinke and J. M. Bowman, in *Molecular Collision Dynamics*, edited by J. M. Bowman (Springer, Berlin, 1982), Chap. 3.
- ⁶⁰S. Bosanac, *Phys. Rev. A* **22**, 2617 (1980).
- ⁶¹F. J. Aoiz, J. E. Verdasco, V. J. Herrero, V. S. Rabanos, and M. H. Alexander, *J. Chem. Phys.* **119**, 5860 (2003).